Injectable bio-responsive hydrogel for therapy of inflammation related eyelid diseases

Liangbo Chen [a,b,1], Dan Yan [a,b,1], Nianxuan Wu [a,b], Qinke Yao [a,b], Hao Sun [a,b], Yan Pang [a,b,*], Yao Fu [a,b,**]

[a] Department of Ophthalmology, Shanghai Ninth People's Hospital, Shanghai Jiao Tong University School of Medicine, Shanghai, China
[b] Shanghai Key Laboratory of Orbital Diseases and Ocular Oncology, Shanghai, China

ARTICLE INFO

ABSTRACT

Eyelid plays a vital role in protecting the eye from injury or infection. Inflammation related eyelid diseases, such as blepharitis, are the most common ocular disorders that affect human's vision and quality of life. Due to the physiological barriers and anatomical structures of the eye, the bioavailability of topical administrated therapeutics is typically less than 5%. Herein, we developed a bio-responsive hydrogel drug delivery system using a generally recognized as safe compound, triglycerol monostearate (TG-18), for in-situ eyelid injection with sustained therapeutics release. In vitro, drug release and disassembly time of Rosiglitazone loaded hydrogel (Rosi-hydrogel) were estimated in the presence or absence of MMP-9, respectively. Moreover, the disassembly of TG-18 hydrogel was evaluated with 9-month-old and 12-month-old mice in vivo. Owing to the bio-responsive nature of Rosi-hydrogel, the on-demand Rosiglitazone release is achieved in response to local enzymes. These findings are proved by further evaluation in the age-related meibomian gland dysfunction mice model, and the bio-responsive hydrogel is used as an in-situ injection to treat eyelid diseases. Taken together, the in-situ eyelid injection with sustained drug release opens a window for the therapy of inflammation related eyelid diseases.

1. Introduction

The eye is the most important sensory organ of the body because approximately 80% of all sensory input is received via the eyes [1]. Eyelids are of paramount importance in protecting the ocular surface from various insults [2]. Eyelid diseases, such as inflammation [3], position and function abnormalities [4], congenital abnormalities [5] and tumors [6], can affect the shape and function of eyelids, thereby leading to ocular surface diseases. Inflammation related eyelid disease such as blepharitis is the most common ocular disorders observed by ophthalmologists [7,8]. In a survey carried out by ophthalmologists in the United States, 37-47% of the patients showed evidence of blepharitis [9]. Hitherto, topical drug administration such as eye drops or ointments is the most common therapy for treating inflammation related eyelid diseases [10]. However, delivering therapeutics to the ocular surface is challenging for multiple reasons, such as fast clearance of eye drops from

the ocular surface and limited drug penetration due to the eyelid or conjunctival barriers [11,12]. Moreover, excessive therapeutics would be absorbed by the eye ball, leading to inevitable drug toxicity. Usually, the bioavailability of the common ophthalmic solution is less than 5% [13,14], resulting in repeated eye drops administration for a long period, which might bring about toxic side effects, such as intraocular hypertension, dry eye, and chronic allergy [15–17]. Therefore, high efficacy, low side effects and alternative administration methods to treat eyelid diseases are significant.

Recently, in order to improve therapeutic efficacy, several drug delivery systems have been developed to administer various drugs and release them in an adjustable manner [18,19]. Among the various drug delivery systems, stimuli-responsive hydrogels have been widely studied for their notable properties, such as 3D structure, high biocompatibility, similarity to living tissues and tunable physical characteristics [20–22]. Therefore, injectable hydrogels have been applied for the treatment of

several ocular diseases [23–25]. However, despite their promise for sustained drug release, few studies have been carried out on the treatment of eyelid diseases. Triglycerol monostearate (TG-18) is a small-molecule amphiphile and recognized as safe (Generally Recognized as Safe, GRAS) compound by Food and Drug Administration (FDA). It can be simply self-assembled during the heating/cooling process [26] to develop hydrogels that encapsulate a wide range of therapeutics and deliver drugs in response to enzymes. Hence, we speculated that TG-18 hydrogel is suitable for therapy of inflammation related eyelid diseases. Herein, we developed the injectable bio-responsive hydrogel using TG-18 and evaluated the therapeutic efficacy of in-situ eyelid injection in age-related meibomian gland dysfunction (ARMGD) mice model. Rosiglitazone is selected as a payload for its function in regulating lipid metabolism as well as anti-inflammatory property [27–30]. We demonstrated the inflammation response properties in vitro through a drug release study with or without matrix metalloproteinase nine (MMP-9), and further confirming it by monitoring hydrogel disassembly in vivo using 9-month-old and 12-month-old mice. Moreover, we proved that Rosi-hydrogel is stable and could sustain the release of the encapsulated therapeutics for 1 month. Furthermore, the in-situ eyelid injection of Rosi-hydrogel using a microinjection needle (27 G) every two weeks successfully delayed the meibomian glands (MGs) atrophy and maintained their biological function in the mice model during aging. Taken together, we speculated that in-situ eyelid injection using bio-responsive hydrogel is a promising therapy for treating inflammation related eyelid diseases in the future.

2. Materials and methods

2.1. Study design

The bio-responsive injectable hydrogel was fabricated, and a potential therapeutic was loaded through a self-assembly process. Drug release, hydrogel disassembly and biocompatibility of the injectable hydrogel were investigated. Subsequently, the in vivo therapeutic effect was evaluated using the mice model. The MGs of 12-month-old mice had been reported to exhibit aged pathological changes [31,32]. Thus, 9-month-old mice (n = 60) (Charles River, China) were raised for 3 months to simulate the aging process, and randomly divided into four groups: Control group (no intervening measure, n = 15), Blank Gel group (injection of 5 μL blank gel under the skin of upper eyelid every two weeks, n = 15), ROSI group (10 mg/kg, oral gavage, once daily, n = 15) and ROSI Gel group (injection of 5 μL Rosi-hydrogel under the skin of upper eyelid every two weeks, n = 15). Four groups were further subdivided into three time points (1 M, 2 M and 3 M after the first intervention, M = months). At each time point, five mice of each group were sacrificed and examined. All animal studies were carried out according to the National Institutes of Health (NIH) guidelines for animal use and in accordance with the Association for Assessment and Accreditation of Laboratory Animal Care. The protocols were approved by the Animal Ethics Committee of Shanghai Jiao Tong University. Mice were allowed free access to standard rodent chow and water, housed under standard 12 h light/dark cycles.

2.2. Reagents

Triglyceride monostearate (TG-18) was purchased from AK Scientific (USA). Rosiglitazone (R2408) (molecular weight: 357.43 g/mol) and matrix metalloproteinase nine (MMP-9) (PF024) were purchased from Sigma-Aldrich (St. Louis, MO, USA). Rabbit anti-NF-κB (Cat#8242), mouse anti-p-NF-κB (Cat#3036) and rabbit anti-GAPDH (Cat#5174) were from Cell Signaling Technology (Danvers, MA, USA). Mouse anti-adiponectin (ab22554) and rabbit anti-PPARγ (ab59256) were from Abcam (Cambridge, UK). Mouse anti-cytokeratin 14 (sc-53253) was from Santa Cruz Biotechnology (CA, USA). Rabbit anti-MMP-3 (GB11131) and anti-MMP-9 (GB11132) were from Servicebio (Wuhan,

China). LIVE/DEAD® Kit Contents Viability/Cytotoxicity Assay Kit (L3224), Alexa Fluor 594-conjugated IgG (A11058), Alexa Fluor 488-conjugated IgG (A11055, A21206), 1,1′-Dioctadecyl-3,3,3′,3′-Tetramethylindodicarbocyanine Perchlorate (DiD) (D307) and BCA protein assay kit (23225) were from Thermo Fisher Scientific (USA). 40,6-diamidino-2-phenylindole (DAPI, H-1200) was from Vector (Burlingame, CA, USA). Quantibody Mouse Cytokine Array 2 was from Ray Biotech (Norcross, GA, USA).

2.3. Preparation of Blank hydrogel and drug encapsulation

In order to fabricate Blank hydrogel (10% w/v), 1 g of TG-18 was weighed into a glass scintillation vial and then 10 mL of DMSO-water mixture (1: 4 vol ratio) was added. The vial was heated to 65 °C for 15 min until TG-18 was dissolved and then placed on a flat surface to allow it to cool to room temperature for 10 min, resulting in hydrogel formation. Rosi or DiD was added to the vial together with TG-18, for a final concentration of 10 mg/mL Rosi and 100 μg/mL DiD.

2.4. Characterization of Blank hydrogel and Rosi-hydrogel

Hydrogel micromorphology was observed by scanning electron microscopy (SEM, Zeiss Merlin Compact). The hydrogel was lyophilized by freeze-drying, followed by sputter-coating with gold at 30 mA for 20 s before observation. The rheological properties were measured on a rheometer (HAAKE MARS60, Thermo-Fisher, Hampton). The variation in the storage modulus (G') and loss modulus (G'') from 65 °C to 25 °C was measured at a fixed frequency of 1 Hz and a heating/cooling rate of 5 °C/min. Frequency sweep experiments were carried out in a frequency range of 0.1–100 rad/s at 25 °C and 0.1% strain. For injectable feasibility, the viscosity of both Blank hydrogel and Rosi-hydrogel was measured before and after injection with the microneedles at 25 °C in a frequency range of 0.1–100 rad/s.

2.5. In vitro release in response to MMP-9

The bio-responsive release of Rosi from Rosi-hydrogel was facilitated at 37 °C and pH 7.4. Rosi-hydrogel (50 μL, 10 mg/mL) was placed in the dialysis tubing (3.5 kDa molecular weight cut-off; Shanghai Yuanye Biotechnology) and suspended in PBS (950 μL) with and without recombinant human MMP-9 (1 μg/mL). MMP-9 was added every 7 days. Subsequently, the dialysis bags filled with Rosi-hydrogels in the release medium were placed in 50 mL sterile PBS, and incubated at 37 °C with agitation at 300 rpm. At each time point, 1 mL sink medium was collected for the detection and replenished with 1 mL fresh PBS to ensure constant sink conditions. The Rosi contents were determined by high-performance liquid chromatography (HPLC) (column: Welch Ultimate Plus - C18, 250×4.6 mm; mobile phase A: 0.02 M ammonium acetate solution; mobile phase B: 100% acetonitrile; flow rate: 1.0 mL/min; temperature: 35 °C; DAD detector: 245 nm).

2.6. Hydrogel disassembly in vitro

The disassembly of hydrogel was investigated by enzymatic disassembly experiments in vitro. Aliquots of Blank hydrogel (200 μL) were added to the upper chambers of the 12-well trans-well plate on Day 0. Chambers were immersed in 1 mL PBS with or without MMP-9 (1 μg/mL). MMP-9 was added every 7 days, and the plates were incubated at 37 °C for 30 days. The weight of the hydrogel was recorded at predetermined time points. The disassembly percentage was calculated through the following equation: Disassembly (%) = W_0-W_t/W_0 × 100%. In this equation, W_0 and W_t were the initial and final weights of the hydrogel after disassembly.

2.7. Hydrogel disassembly in vivo

9-month-old and 12-month-old mice were injected with TG-18 hydrogel loaded with DiD (5 μL, 100 μg DiD/mL) under the skin of the upper eyelid on Day 0. Every other day for 14 days, mice were anesthetized via isoflurane inhalation and subsequently imaged using an in vivo imaging system (IVIS).

2.8. Isolation and culture of primary mouse meibocytes

The preparation of primary mouse meibocytes was described in a previous study [33]. Briefly, the upper and lower eyelids of twenty 4-week-old mice were removed, disinfected with 75% ethanol, and dissected under a Zeiss microscope. The tissues were washed with PBS and placed in Dulbecco's modified Eagle's medium (DMEM) supplemented with 100 U/mL penicillin/streptomycin (Gibco, USA). After the conjunctiva and excess skin were removed, the tarsal plates were placed in DMEM containing 0.25% collagenase A (Invitrogen, Carlsbad, CA) and 0.6 U/mL dispase II (Invitrogen). Then, the glands were digested at 37 °C for 6 h, followed by centrifugation at 1000 rpm for 10 min. Subsequently, the cell pellet was suspended in keratinocyte growth medium (KGM, Lonza Walkersville, Inc., Walkersville, MD, USA) containing human epidermal growth factor (hEGF), hydrocortisone, insulin and gentamicin and supplemented with 10% fetal bovine serum (FBS). Cells were cultured in 6-well plate in a humidified atmosphere with 5% CO_2 at 37 °C.

2.9. In vitro biocompatibility

Viability staining was performed using Live/Dead™ assay, as described previously [34]. Briefly, 5×10^4 primary mouse meibocytes (Passage 2) were seeded in 24-well plates (Corning) containing trans-well inserts (Millipore, USA). After culturing overnight, medium was replaced with fresh medium, fresh medium with 50 μL Blank hydrogel and fresh medium with 50 μL Rosi-hydrogel was added to the upper chamber. After 48 h of incubation, the culture medium was aspirated, and the cells were rinsed with PBS twice. Subsequently, meibocytes were incubated in PBS containing ethidium homodimer 2 (EthD-2) and calcein-acetoxymethylester (CAM) at 37 °C for 15 min. Live (green stain) and dead (red stain) cells were captured using a fluorescence microscope (Olympus BX51; Olympus, Tokyo, Japan). Finally, the cell viability was quantified by dividing the number of dead cells by the total number of cells.

2.10. Morphology of MGs and corneal fluorescent staining (CFS)

All mice were weighed before experiments. Before capturing, 1 μL of 1% liquid sodium fluorescein (Jingmingxin Co., Ltd., Tianjin, China) was dropped into the conjunctival sac, and CFS was captured after 60 s later under the slit-lamp microscope with a cobalt blue filter. The cornea was divided into four quadrants and graded as follows: 0 point for no staining; 1 point for mild punctate staining; 2 points for moderate punctate staining (between 1 and 3 points); and 3 points for the existence of filamentary keratitis or piece staining. The total score was obtained by adding the score of the four quadrants (0–12). Mice were sacrificed, and the upper and lower eyelids were excised through a Zeiss microscope. The structure of MGs was clinically photographed with a Keratograph (Oculus, Wetzlar, Germany). The score of MGs was evaluated according to clinical standards: 0 point for no disordered MGs or MGs dropout; 1 point for disordered MGs, but no MGs dropout; 2 points for disordered MGs with MGs dropout, but, the loss of MGs is less than 1/3; 3 points for disordered MGs with MGs dropout and the loss is greater than or equal to 1/3. The scores of MGs were assessed based on the photographs and data presented as mean ± SD.

2.11. Histology

Eyelid tissues from four groups were collected and embedded in optimal cutting temperature (OCT) compound or paraffin, followed by slicing into sagittal sections (8-μm-thick). Frozen sections were stored at −80 °C, and paraffin sections were stored at room temperature. Hematoxylin and eosin (H&E) staining was performed on paraffin sections, while immunofluorescence staining and Oil Red O were performed on frozen sections.

2.12. Oil Red O staining

Frozen eyelid sections were fixed in 4% paraformaldehyde for 15 min and washed in PBS for 5 min, followed by staining with freshly prepared Oil Red O solution for 10 min. The sections were counterstained with hematoxylin and mounted in 90% glycerol.

2.13. Immunofluorescence staining

Frozen sections were fixed in cold acetone (−20 °C) for 15 min, permeabilized with 0.3% Triton X-100 for 30 min, blocked with 5% donkey serum in PBS for 1 h at room temperature, and incubated with MMP-3 (1:200), MMP-9 (1:200), NF-κB p65 (1:200), phosphor NF-κB p65 (1:200) and PPARγ (1:200) antibodies overnight at 4 °C. Negative control was incubating the sections without primary antibody. The sections were then incubated with Alexa Fluor 488-conjugated IgG (1:400) or/and Alexa Fluor 594-conjugated IgG (1:400) for 1 h at room temperature, followed by counterstaining with DAPI. The images were acquired by fluorescence microscopy (Olympus BX51, Olympus, Tokyo, Japan). The average intensity of fluorescence staining was measured through Image J software. Meibocytes were immunofluorescence stained with PPARγ (1:200) and Cytokeratin 14 (1:100).

2.14. Western blot analysis

Isolated MGs were stored at −80 °C overnight, subsequently extracted in lysis buffer containing phosphatase and protease inhibitors. The protein concentration was measured using the BCA protein assay kit. Three samples were used from each group. An equivalent of 30 μg protein extract was subjected to electrophoresis on 10% Tricine gel and transferred to PVDF membranes (0.22 μm). Then, the membranes were blocked in 5% BSA for 60 min and incubated with PPARγ (1:1000), phospho-NF-κB (1:1000) and GAPDH (1:5000) antibodies overnight at 4 °C. The data were observed using an Odyssey V 3.0 image scanner (LI-COR) after incubation with DyLight TM680-conjugated secondary antibodies (1:10000, Sigma).

2.15. Quantification of mouse cytokine using an antibody array

MGs protein extracts were collected as mentioned above. The concentrations of six selected inflammatory cytokines were measured using a Quantibody Mouse Cytokine Array. The cytokines array was carried out as previously reported [35]. Tissue samples were detected using a GenePix scanner (Axon Instruments Inc., Foster City, CA, USA) and further analyzed using GenePix Pro 6.0 software (Axon Instruments Inc.).

2.16. Enzyme-linked immunosorbent assay (ELISA)

Three 9-month-old mice and three 12-month-old mice were used in this experiment. MGs from each mouse were lysed in 100 μL RIPA lysis buffer in the presence of protease inhibitors (Roche), and the level of MMP-9 protein was detected using an ELISA kit. All samples were assayed in three technical replicates. Data represented as mean ± SD.

2.17. Statistical analysis

Data were processed using GraphPad Prism 7.0 software (GraphPad Software Inc, San Diego, CA, USA). At least three samples were tested for each experiment, and data are presented as means ± SD (*P < 0.05, **P < 0.01 and ***P < 0.001). Multiple t-tests using a false discovery rate approach (two-stage step-up method of Benjamini, Krieger, and Yekutieli) was conducted to analyze the differences between the two groups. P < 0.05 indicated statistical significance.

3. Results and discussions

3.1. Preparation of injectable Rosi-hydrogel and research scheme

Injectable Rosi-hydrogel was fabricated with simple procedures, as reported previously using GRAS compound TG-18. A schematic of the hydrogel formation and enzyme-responsive drug release is illustrated in Fig. 1. TG-18 consists of a hydrophobic tail (polymethylene) and a hydrophilic head group (polyhydroxyl). Upon heating to 65 °C in a dimethyl sulfoxide/water mixture, TG-18 forms a clear solution due to the formation of micelles. The subsequent cooling results in a solid hydrogel due to self-assembly (Fig. S1), and the hydrophobic compounds can be encapsulated into the hydrophobic core of the TG-18 hydrogel. The Rosi-hydrogel was injected subcutaneously, and residing nearby the MGs region for sustained release of Rosi. Furthermore, MMP-9 around the MGs accumulates during the aging process, thereby accelerating the disassembly of Rosi-hydrogel and enhancing Rosi release, which in turn suppressed the secretion of MMP-9 accompanied by slow release of Rosi to maintain a long-term therapeutic effect.

3.2. Morphology and rheological properties of hydrogels

SEM was applied to evaluate the surface morphology of the Blank hydrogel and Rosi-hydrogel. Representative SEM images of lyophilized Blank hydrogel and Rosi-hydrogel were shown in Fig. 2a and 2b. The lamellar structures were observed in Blank hydrogel, and when Rosi was loaded into the hydrophobic core, higher-order fibrous assemblies were obtained, which proved successful encapsulation of Rosi. The

rheological properties of Blank hydrogel at different concentrations (5%, 10%, 20% and 30% w/v) were monitored by rheometer (Fig. 2c and Fig. S2), and 10% w/v was chosen for further study. As the temperature decreased from 65 °C, the storage modulus G' increased rapidly, the gelation temperature (G' = G'') was 58.21 °C for the Blank hydrogel (Fig. 2c) and 60.78 °C for Rosi-hydrogel (Fig. 2d). Thus, it could be suggested that the sol-gel transition occurs at approximately 60 °C. The frequency sweep measurements demonstrate that both Blank hydrogel and Rosi-hydrogel exhibited G' values increased 3-4 times throughout the frequency sweep from 0.1 to 100 rad/s and remained much greater than the G'' values, indicating the formation of stable hydrogels (Fig. 2e and f). The shear viscosity frequency sweep measurement further confirmed the injection feasibility of the obtained gel (Fig. 2g). It was found that no matter the Blank hydrogel or the Rosi-hydrogel showed a decrease in the viscosity after injection throughout the frequency sweep from 0.1 to 100 rad/s, which verified the shear thinning characteristic of the hydrogel and the hydrogel could pass through the microneedles easily.

3.3. Drug release, disassembly and biocompatibility of Rosi-hydrogel

MMP-9 is a crucial gelatinase present on the ocular surface [36], and desiccating stress is a non-negligible reason for the elevated MMP-9 in a murine model [37]. Herein, the cumulative release of Rosi in response to MMP-9 in vitro was investigated. Rosi-hydrogel was incubated in phosphate-buffered saline (PBS) (pH 7.4) at 37 °C with or without MMP-9 (1 μg/mL). In the absence of MMP-9, Rosi-hydrogel demonstrated excellent stability in PBS, with only approximately 5% release of Rosi within 24 h and 30% cumulative release of Rosi over 30 days. This proved that Rosi-hydrogel was stable at normal condition, and thus, the therapeutics encapsulated in the hydrogel did not burst release and led to drug toxicity. Repeated addition of MMP-9 every 7 days significantly increased the cumulative drug release from 30% to almost 50% on day 30. The total drug release of the MMP-9 group was 1.47-fold compared to the control group (Fig. 2h). Subsequently, we tested the disassembly rate of the Rosi-hydrogel in vitro under cell-mediated condition by monitoring the hydrogels' residual weight (Fig. 2i). The weight of the Rosi-hydrogel incubated with PBS was heavier on day 3 than on day 0. We speculated that the swelling rate of the hydrogel was dominant
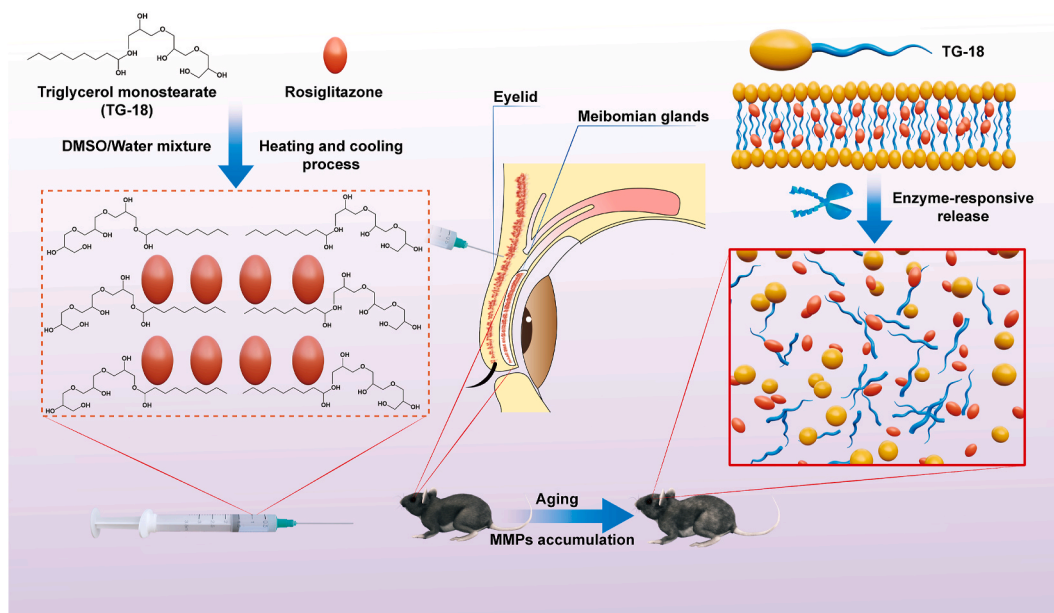

Fig. 1. Schematic illustration of hydrogel formation and Rosi release for treating ARMGD. TG-18 could gelation through self-assembly with model therapeutic rosiglitazone encapsulated. TG-18 hydrogel was injected under the eyelid skin near the MGs area. With aging, MMPs accumulated in the MGs area, thus accelerating hydrogel disassembly and Rosi release for treating ARMGD.
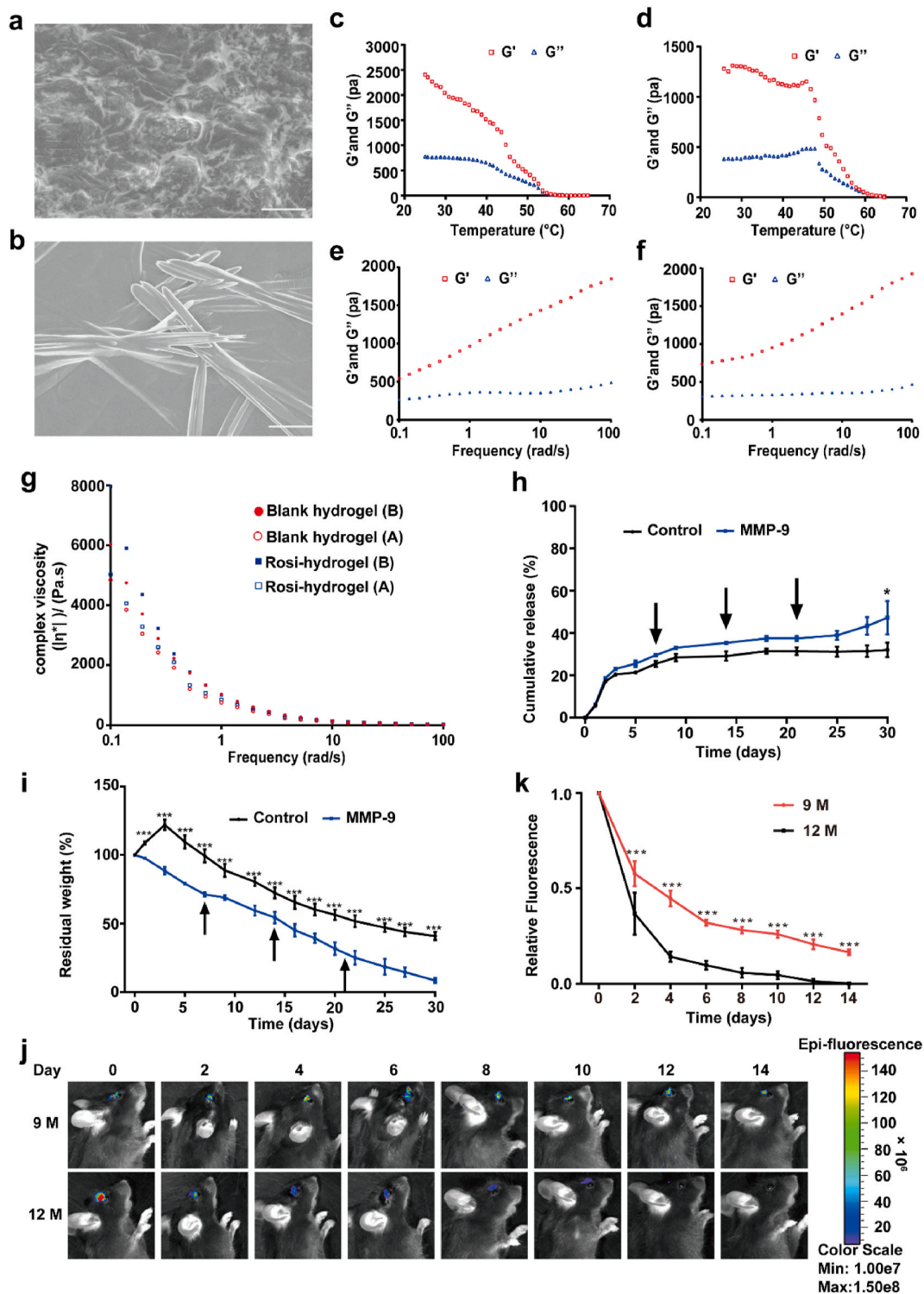
Fig. 2. Characterizations of the injectable hydrogels. (a, b) SEM of Blank hydrogel and Rosi-hydrogel (Scale bar: 10 μm). (c, d) Temperature sweeps of (c) Blank hydrogel and (d) Rosi-hydrogel. Sweeps were performed at a fixed frequency of 1 Hz and a heating/cooling rate of 5 °C/min (e, f) Frequency sweeps of (e) Blank hydrogel and (f) Rosi-hydrogel. Sweeps were performed at 0.1% strain and 25 °C. (g) Gel viscosity of the Blank hydrogel and Rosi-hydrogel before and after injection with the microneedles with a shear rate ranging from 0.1 to 100 rad/s at 25 °C. Abbreviations: B, before injection; A, after injection. (h) In vitro release kinetics of Rosi from Rosi-hydrogel in PBS at 37 °C with or without MMP-9 (*P < 0.05 and **P < 0.01). (i) Disassemble rate of the Rosi-hydrogel in vitro. At each determined time point, the residual weight percentage of the control group was significantly higher than the MMP-9 group. Error bars represent SD (n = 3). ***P < 0.001. (j) Degradation of the DiD-loaded TG-18 hydrogel was evaluated in 9-month-old and 12-month-old mice. Representative IVIS images were captured every 2 days for 2 weeks. (k) Relative fluorescence (normalized to Day-0) was measured. Hydrogel disassembly significantly faster in 12-month-old mice than in 9-month-old mice (***P < 0.001).

compared with the degradation rate in the initial stage, so the weight of the hydrogel kept increasing until it reached the summit. Following, the hydrogel degraded by about 30% on day 14 and about 59% on day 30, confirming that the hydrogel had good stability under normal conditions. However, when the hydrogel was incubated with MMP-9, the disassemble rate increased greatly, the hydrogel degraded by about 44% on day 14, and about 90% on day 30. At each determined time point, the residual weight of the hydrogel incubated with PBS was significantly higher than that with MMP-9. Thus, in the presence of MMP-9, Rosi-hydrogel disassembled faster and released more Rosi in vitro. Enzymes, including MMPs can cleave the ester bonds in the TG-18 hydrogel and accelerate the release of encapsulated drugs. We also investigated the hydrogel disassembly rate in vivo using 9-month-old and 12-month-old mice. Through using the commercially available ELISA kit, the protein level of MMP-9 was quantitatively analyzed. The average concentration of MMP-9 in 12-month-old mice MGs was 61.47 ng/mL, which was significantly higher than that in 9-month-old mice MGs (Fig. S3). The data demonstrated that aging would lead to an increase in MMP-9 around the MGs region. Subsequently, a volume of 5 μL of fluorescent dye 1,1′-Dioctadecyl-3,3,3′,3′-Tetramethylindodicarbocyanine Perchlorate (DiD)-loaded Blank hydrogel was injected under the eyelid skin of mice on Day 0. DiD is a hydrophobic dye that is retained within the hydrogel until enzymes degrade the hydrogel. Subsequently, the mice were imaged using an IVIS every alternate day. The hydrogel fluorescence signal decreased to about 32% of the initial signal intensity under the eyelid skin of 9-month-old mice on day 6, and 16% on day 14. On the contrary, in 12-month-old mice, the fluorescence signal decreased to about 10% of the initial on day 6, and it was negligible by day 14. The relative fluorescence signal was significantly higher in the 9-month-old mice than in the12-month-old mice at each determined time point (Fig. 2j and k). The change of the fluorescence signal can partially reflect the disassembly of the hydrogel in vivo. The degradation of the hydrogel in vivo was faster than when it was incubated with PBS in vitro. We speculated that there are various enzymes in vivo, which will accelerate the degradation of the hydrogel. In addition, with aging, local enzymes such as MMP-9 accumulated around the MGs region, which would further accelerate the disassembly of the hydrogel.

TG-18 hydrogel is crosslinked by ester bonds. Reportedly, the Zn (II) ion of MMPs can bind to the external water molecules, followed by deprotonation. Subsequently, the formation of Zn (II)-bond hydroxides acts as nucleophiles and attack the ester bonds in the TG-18 hydrogel [38,39]. Accompanied by the breaking of ester bonds, the Rosi-hydrogel disassembled, and the loaded hydrophobic drug Rosi was released. MMPs-responsive drug delivery systems have been developed before via the synthesis of specific MMP-cleavable peptide, such as GGRMSMPV [40], which is connected through chemical conjugation. Supposedly, the approach of TG-18 hydrogel formation does not require complex chemical modification and can be self-assembled through temperature modification. In vitro and in vivo experiments have proved that MMP-9 can significantly promote the disassembly of TG-18 hydrogel and the release of the encapsulated drugs. Considering that ARMGD is accompanied by an increase of MMP-9 around the MGs region, this drug delivery platform is suitable for ARMGD therapy. Importantly, TG-18 hydrogel can encapsulate a large range of therapeutics. For example, Gajanayake et al. demonstrated the practicability of TG-18 for the local delivery of tacrolimus in a model of vascularized composite allotransplantation [41]. Moreover, Joshi et al. loaded triamcinolone acetonide in TG-18 hydrogel for treating inflammatory arthritis [42]. In both in vivo and in vitro experiments, TG-18 hydrogel showed obvious enzyme responsiveness, which has great advantages in treating models with elevated esterases. Typically, TG-18 hydrogel interacts with various hydrophobic therapeutics and exhibits translational potential in treating multiple inflammation related ocular diseases, including MGD, in the future.

Subsequently, we investigated the biocompatibility of the Blank hydrogel as well as Rosi-hydrogel. Primary mouse meibocytes were identified through morphology and two positive biomarkers of meibocytes, namely PPARγ and Cytokeratin 14 (Fig. S4). Subsequently, primary meibocytes (passage 2) were incubated in a 24-well-transwell plate in medium, medium with Blank hydrogel or Rosi-hydrogel added in the upper chamber. After 48 h incubation, live/dead staining didn't show significant changes in cell morphology or viability loss in all three groups (Fig. 3a and b). Furthermore, after injection, the MGs sections were stained with H&E to evaluate the in vivo toxicity. Hydrogel injection every two weeks did not lead to the influx of inflammatory cells around the MGs area for 3 months (Fig. 3c). Moreover, no significant difference was detected in the bodyweight of mice of each group (Fig. S5), and both hydrogels did not cause lesions in various organs (heart, liver, spleen, lung, and kidney) of the mice, proving that this drug delivery system had no obvious toxicity to the mice (Fig. S6).

3.4. In vivo therapeutic efficacy evaluation of Rosi-hydrogel

A total of 59% of older adults (average age, 63 years) suffer from at least one symptom of meibomian gland dysfunction (MGD), such as dryness, itching, foreign body sensation and even blurred vision [43–46]. MGs dropout and plugging of MGs orifice are pivotal clinical signs of MGD [47,48]. Mice were sacrificed, and the upper eyelids were collected for evaluating the morphology of MGs. Yellow arrows indicate disordered MGs, while red arrows indicate MGs dropout. An injection schematic was carried out, as shown in Fig. 4a. Mice with disordered MGs and MGs dropout increased in the Control and Blank Gel groups with aging. Conversely, mice in the ROSI and ROSI Gel groups showed relatively integral MGs during aging (Fig. 4b). The upper eyelids of all mice from each group were evaluated and scored, respectively (Fig. 4c). The mean clinical MGs score for each group was shown in Table S1. It was discovered that the mean MGs score of the Control group increased obviously during aging (0.8 ± 0.632, 1.3 ± 1.059, and 1.6 ± 0.966 for 1 M, 2 M, and 3 M, respectively). On the contrary, under Rosi-hydrogel treatment, the mean MGs score increased slightly during aging (0.5 ± 0.527, 0.6 ± 0.699, and 0.8 ± 0.632 for 3 months, respectively). At each time point, the mean MGs score of mice in the Control and Blank Gel groups was higher than that in the other two groups. This proved that Rosi, whether administered systemically or locally by hydrogel injection, could delay the atrophy of MGs during the aging process of mice.

Frozen upper eyelid sections were stained with Oil Red O staining buffer to demonstrate the lipids inside the MGs (Fig. 4d). MGs area without lipid staining increased during aging in the Control and Blank Gel groups; however, this phenomenon was not detected in the other two groups. Single MG area was measured using Image J software, and a significant decrease was noted with aging in the Control group. On the contrary, mice in the ROSI Gel group showed a relatively larger MG area as compared to the mice in the Control and Blank Gel groups at the three time points (Fig. 4e).

CFS is a major evaluation indicator for the MGs' biological functions, as described previously [49–51]. As shown in Fig. 4f, unlike the ROSI and ROSI Gel group, mild punctate staining or moderate punctate staining was observed in the Control and Blank Gel groups at 1 M. Consecutively, more punctate staining or piece fluorescent staining was discovered in the Control and Blank Gel groups during aging. Conversely, in the ROSI Gel and ROSI groups, the cornea of mice did not show significant fluorescent staining until 3 M. The CFS scores of all mice in the four groups were evaluated (Fig. 4g). The CFS scores increased significantly from 1 to 3 months in the Control group. Moreover, the CFS scores of the ROSI Gel group were significantly lower than that of the Control and Blank Gel groups at three time points. A similar treatment effect was observed in the ROSI group as compared to the ROSI Gel group.

In this study, the ROSI group was set up to evaluate the treatment effect of systemic administration of Rosi on the MGs. When analyzing the clinical MGs scores and CFS scores, no significant difference was detected between the ROSI group and the ROSI Gel group at all time
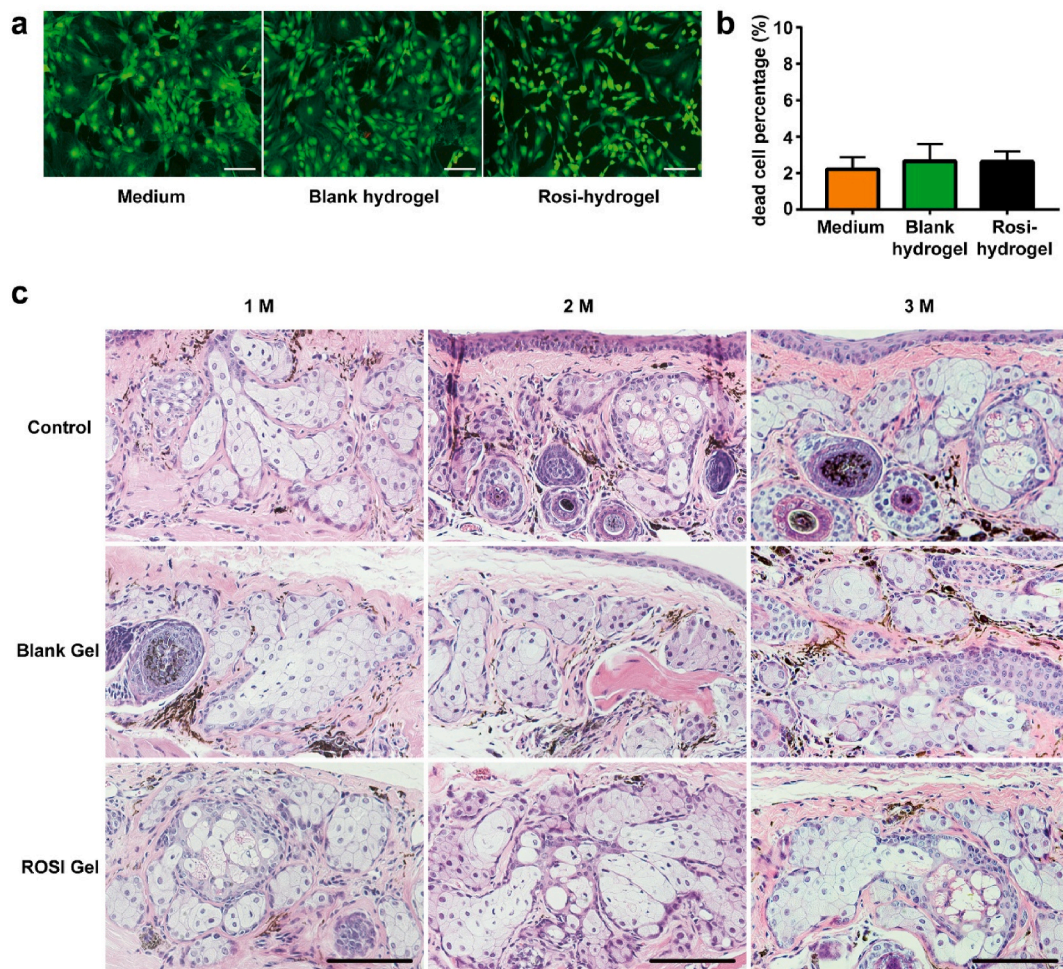
Fig. 3. Biocompatibility of Rosi-hydrogel. (a) Representative fluorescence images after live/dead staining of primary mouse meibocytes incubated for 48 h in medium or medium with Blank hydrogel or Rosi-hydrogel added to the upper trans-well chamber (Scale bar: 200 μm). Green indicated viable cells stained with calcein-AM, whereas red represented dead cells stained with ethidium homodimer-1. (b) Quantification of dead cells according to live/dead staining analysis. No significant difference was detected among the three groups. (c) Representative photomicrographs of MGs sections stained with H&E. Hydrogel injection did not cause the accumulation of inflammatory cells inside the MGs area. M indicates month, Scale bar: 100 μm.

points. The comparison of the ROSI and ROSI Gel groups to the Control and the Blank Gel groups revealed significantly decreased MGs and CFS scores, indicating that both the ROSI and ROSI Gel groups have a similar treatment effect. However, the ROSI Gel group has three advantages over the ROSI group. Firstly, our drug delivery system is a sustained release system, which can ensure sufficient drug concentration for a prolonged period, thus greatly reducing the frequency of treatment. Secondly, local injection improves the bioavailability of therapeutics. The TG-18 hydrogel exhibits excellent enzyme-response characteristic. Both in vitro and in vivo experiments proved that elevated MMP-9 accelerates the degradation of the hydrogel and the release of Rosi, and the released Rosi, in turn, inhibited the secretion of MMP-9. Therefore, we speculated that this feedback could slow down the disassembly of the hydrogel and achieve the purpose of on-demand therapeutic release, which further improves the therapy efficiency of the hydrogel. Finally, topical injection reduces the treatment cost and avoids long-term systemic drug toxicity. The amount of Rosi required for one injection in the ROSI Gel group was 50 μg once, while it was almost 300 μg for the ROSI group per day. The total amount of Rosi required for oral gavage was 84-fold that of local injections. Therefore, Rosi-hydrogel reduces the cost of treatment. Moreover, drugs in the ROSI Gel group were administered locally, instead of systemic administration, which avoided toxic side effects throughout the body. Strikingly, the injectable bio-responsive hydrogel greatly improved the therapeutic efficacy and reduced the cost.

3.5. Sustained release of Rosi maintained expression of PPARγ of MGs during aging

PPARγ plays a vital role in maintaining the terminal differentiation of meibocytes [52] and could suppress the NF-κB pathway [53]. With aging, the expression of PPARγ significantly decreased in the Control and Blank Gel groups (Fig. 5a and b). On the contrary, the expression of PPARγ in the ROSI Gel group was relatively the same after 3 months and was significantly higher than that in the Control group (P < 0.01), and Blank Gel group (P < 0.001) at 3 M. Western blot analysis further confirmed that expression of PPARγ decreased with aging and Rosi treatment could enhance the expression of PPARγ (Fig. 5g). Hitherto, several in vitro studies had proved that Rosi could promote the differentiation and lipid synthesis of hMGECs and primary meibocytes. However, currently, there are no in vivo studies of Rosi on treating ARMGD. Therefore, our study for the first time confirmed that Rosi could maintain the expression of PPARγ during aging in vivo, and thus delaying acinar atrophy and preventing ARMGD.

3.6. Rosi-hydrogel effectively suppressed the NF-κB pathway and inhibited accumulation of inflammatory cytokines

Currently, it is speculated that MGD is accompanied by inflammation [54], and thus inhibition of inflammation is also essential for treating
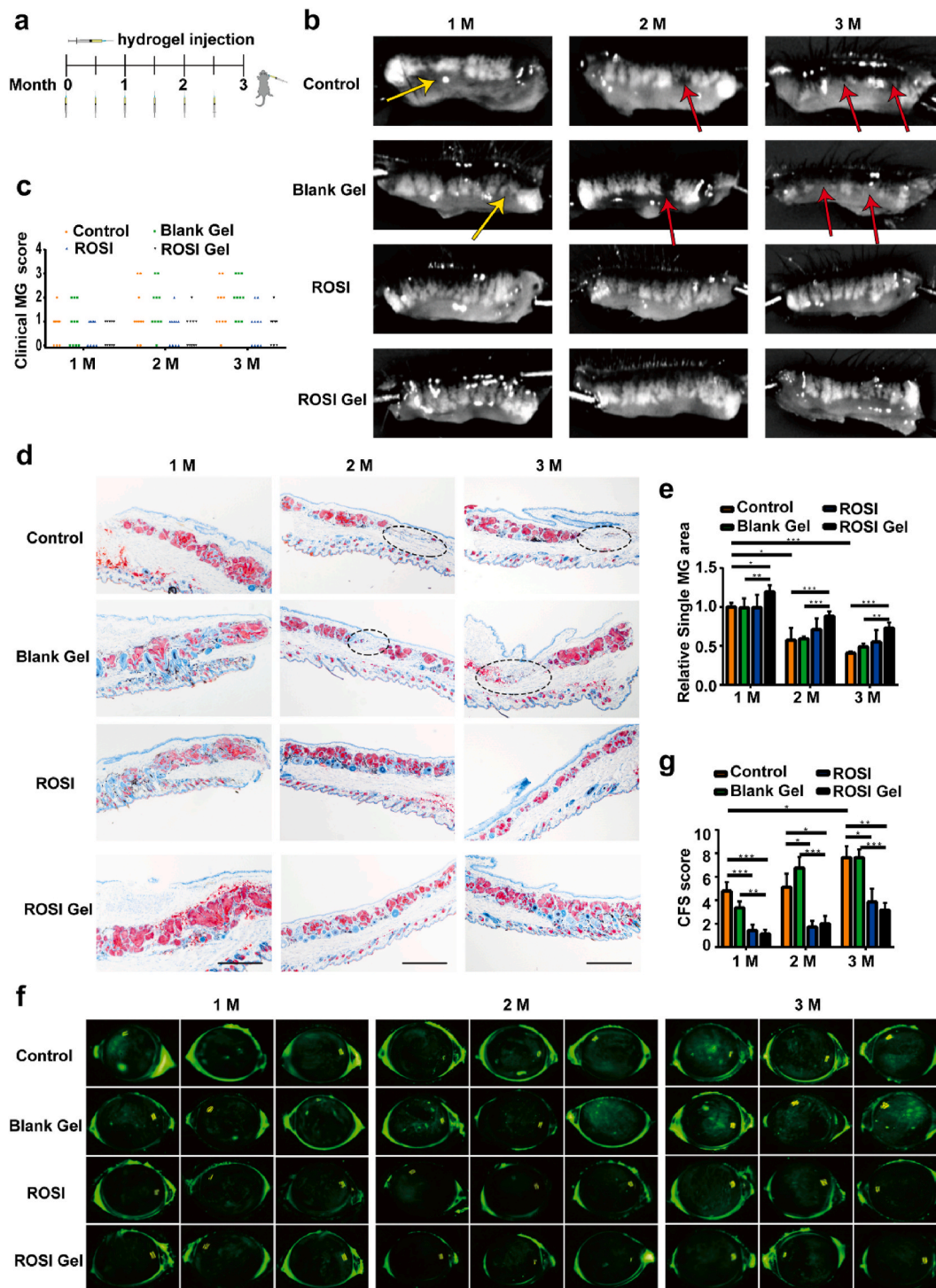
Fig. 4. The therapeutic effect of Rosi-hydrogel on MGs (upper eyelids were harvested for evaluation). (a) Injection schematic: 9-month-old mice were raised for 3 months to simulate the natural aging process. Rosi or Blank hydrogel was injected in proximity to the MGs region every 2 weeks. (b) Representative images of MGs in the four groups at 1 M, 2 M and 3 M after the experiment. The MGs dropout (red arrows) and disordered MGs (yellow arrows) are key clinical signs of MGD. MGs atrophy could be observed in the Control and Blank Gel groups during aging, while no significant difference was detected in the morphology of MGs during aging in the ROSI Gel group. (c) Clinical MGs score of all mice in the four groups for 3 months. (d) Frozen cross-sections of the upper eyelids were stained with ORO staining buffer to show the lipid droplets inside the MGs. The black dotted line indicated the space without MGs. Scale bar: 500 μm. (e) Relative single MG area of the mice in the four groups at three time points. Single MG area was measured through Image J software. Data were evaluated from three sections per each eyelid, with 3 mice in each group. (f) Three representative CFS images from each group. With aging, punctate fluorescent staining or piece fluorescent staining gradually appeared on the cornea of the mice in the Control group. However, no severe fluorescent staining was detected on the cornea of the mice in the ROSI Gel group. (g) Average CFS scores for four groups. The mean CFS score of the ROSI Gel group was significantly lower than that of the Control group at three time points. *P < 0.05, **P < 0.01, ***P < 0.001. M indicates month.
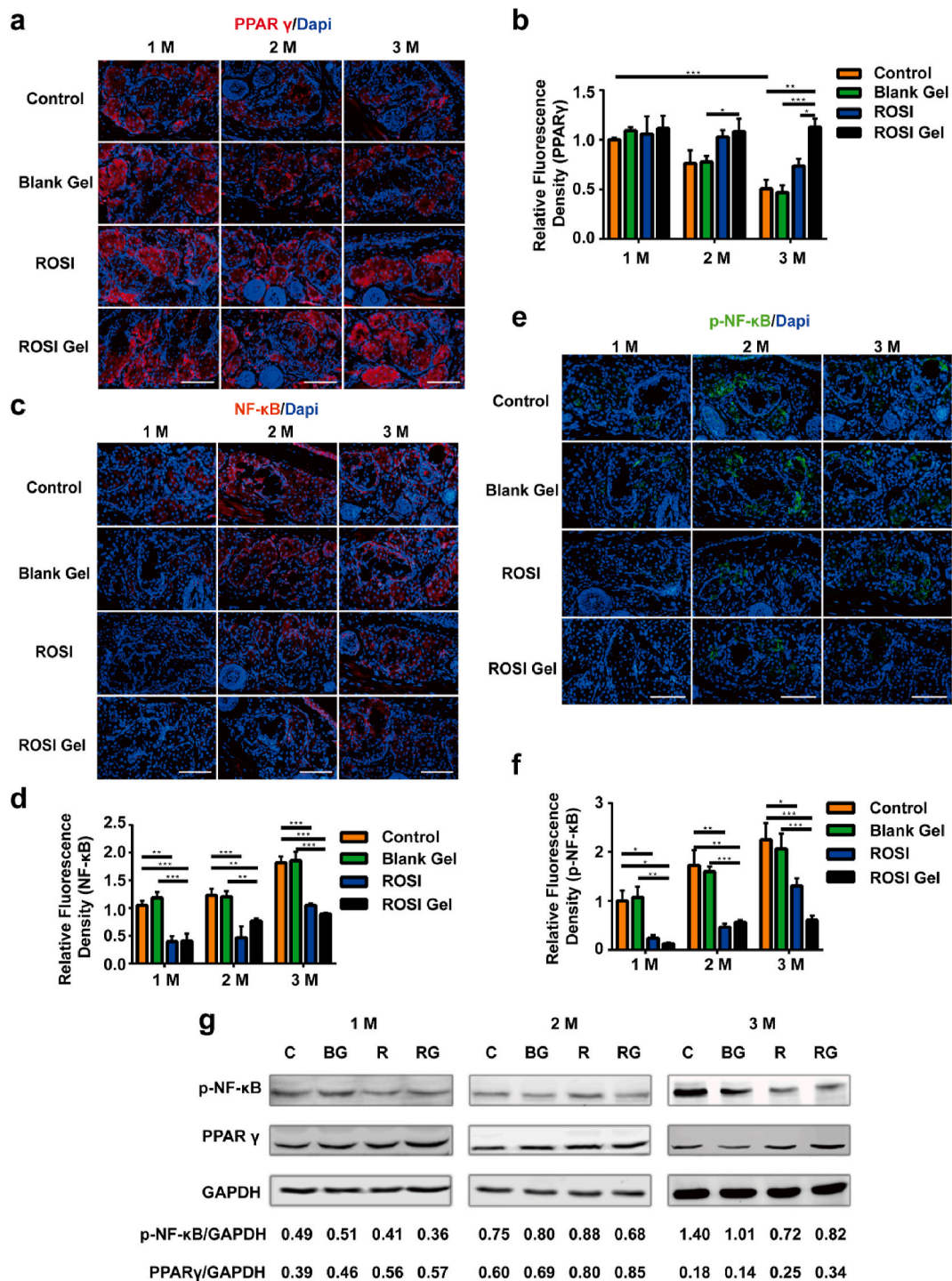
Fig. 5. Rosi-hydrogel treatment increased the PPARγ expression and suppressed the NF-κB pathway. (a, b) Representative immunofluorescent staining images of PPARγ. The decreased immunofluorescent intensity of PPARγ in the Control and Blank Gel groups during aging, a similar trend was not observed in the ROSI Gel group. (c-f) Representative immunofluorescent staining images of NF-κB and p-NF-κB, respectively. During aging, the MGs in the Control and Blank Gel groups showed an increased immunofluorescent intensity of both NF-κB and p-NF-κB. Moreover, the low immunofluorescent intensity of NF-κB and p-NF-κB was discovered in the ROSI and ROSI Gel group. (g) Western blot analysis showed upregulation of PPARγ and down-regulation of p-NF-κB in the ROSI Gel group during aging. C, BG, R, and RG represents the Control, Blank Gel, ROSI, and ROSI Gel groups. Data are shown as mean ± SD. *P < 0.05, **P < 0.01 and ***P < 0.001. M indicates month, Scale bar: 100 μm.

MGD. The NF-κB pathway plays a crucial role in regulating innate immune and inflammatory responses [55,56]. Therefore, immuno-staining and western blot analysis were carried out to investigated the expression of NF-κB and p-NF-κB in the MGs of mice during aging. Compared to the Control group and Blank Gel groups, the expression of both NF-κB and p-NF-κB was significantly downregulated in the ROSI and ROSI Gel groups at all time points (Fig. 5c–f). Western blot analysis demonstrated that the NF-κB pathway was suppressed as well (Fig. 5g).

In order to illustrate the anti-inflammation function of PPARγ, the protein levels of some inflammatory cytokines of the MGs tissues collected from mice were detected using a Quantibody Mouse Cytokine Array. As shown in Fig. 6, six inflammatory cytokines were detected in
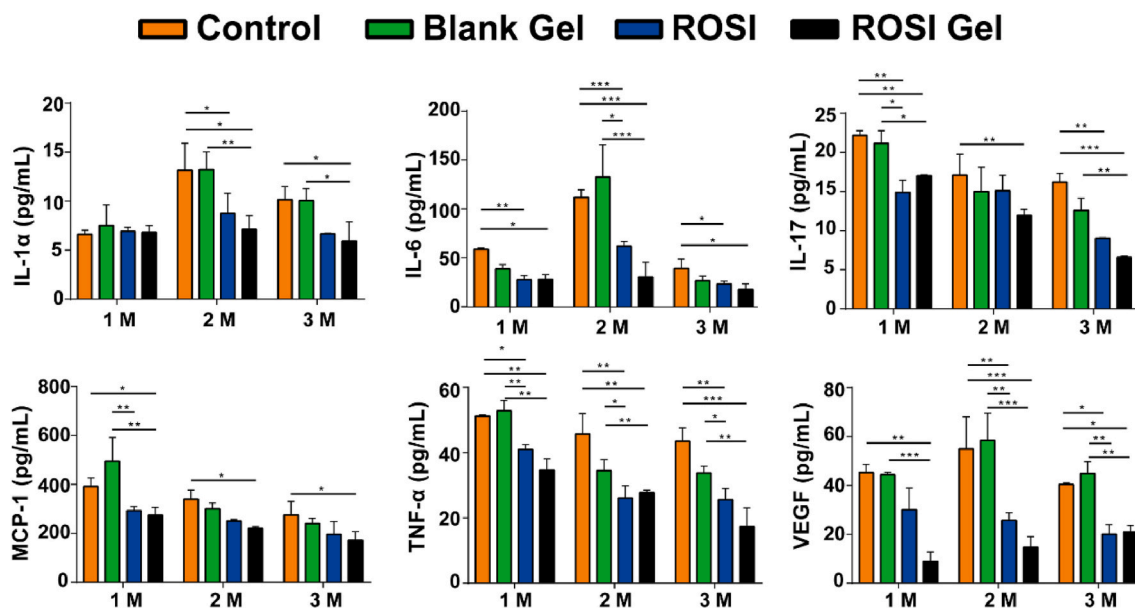
Fig. 6. Rosi-hydrogel treatment attenuated the inflammation of the MGs. Protein levels of 6 inflammatory cytokines in the MGs tissue extracts were detected through a Quantibody Mouse Cytokine Array (n = 3/group). As a response to Rosi-hydrogel treatment, inflammatory cytokines decreased as compared to the Control group. Data are presented as means ± SD, *P < 0.05, **P < 0.01 and ***P < 0.001. M indicates month. Abbreviations: IL, interleukin, MCP, monocyte chemoattractant protein, TNF, tumor necrosis factor, VEGF, vascular endothelial growth factor.

the MGs tissue extracts. Intriguingly, under Rosi-hydrogel treatment, the protein levels of 6 inflammatory cytokines were lower than those in the Control and Blank Gel groups. The protein levels of five cytokines (IL-6, IL-17, MCP-1, TNF-α and VEGF) were significantly lower in the ROSI Gel group than in the Control group at three time points. However, only two cytokines (IL-6 and TNF-α) tested showed a steady decline in the ROSI group compared to the Control group. This proved that Rosi-hydrogel was more effective than Rosi oral gavage in inhibiting MGs inflammation.

3.7. Local release of Rosi reduces MMPs activity

MMPs play essential roles in regulating cell homeostasis in the MGs [57]. Controlling its activity is crucial for the maintenance of ocular surface health, and abnormal activity is associated with inflammation and disease [58]. Therefore, MMPs accumulated in the MGs region during aging could accelerate cleaving the ester bonds inside the hydrogel and releasing the encapsulated Rosi. Thus, the activity of MMP-9 was investigated in this study. At 1 M, low MMP-9 expression was discovered in all four groups, which proved that the activity of MMP-9 in the MGs was relatively low at this time point. A significant increase in the expression of MMP-9 was observed in the MGs region of both the Control and Blank Gel groups during aging. When mice were treated with daily oral gavage Rosi, MMP-9 accumulation could still be observed around the MGs area, although significantly lower than that in the Control group. On the contrary, low-level expression of MMP-9 in the MGs region of the ROSI Gel group was discovered at all three time points, proving that Rosi-hydrogel administration every two weeks could still inhibit the secretion of MMP-9 (Fig. 7a and b). Similarly, Rosi-hydrogel treatment significantly suppressed the secretion of MMP-3 at 3 M (Fig. S7).

4. Conclusions

Inflammation related eyelid diseases are the most common ocular disorders implicated to play a crucial role in many ocular diseases progressing to their advanced stages by disrupting normal ocular surface homeostasis. Topical eye drops administration is the most common

treatments clinically. However, due to the ocular surface barriers, the bioavailability of a common ophthalmic solution is typically less than 5%. In this study, we developed an injectable bio-responsive hydrogel and encapsulated Rosi as a therapeutic model. In vitro and in vivo experiments proved that in the presence of MMP-9, Rosi-hydrogel disassembled faster and released the encapsulated therapeutics more quickly, which proved the bio-responsive characterization of the hydrogel. Subsequently, the ARMGD mice model was chosen to evaluate the therapeutic efficacy of in-situ eyelid injection. Rosi-hydrogel was subcutaneously injected through a microinjection needle (27 G), which was minimally invasive. After Rosi-hydrogel treatment, the atrophy of MGs was delayed, the biological function of MGs was maintained, and ARMGD was effectively prevented. This study firstly introduced the injectable hydrogel into the treatment of inflammation related eyelid diseases. It also proved that retaining the expression of PPARγ in vivo during aging could successfully prevent MGs atrophy. Moreover, since the injectable bio-responsive hydrogel can encapsulate a large range of hydrophobic therapeutics via the simple physical method, it is a promising alternative therapy for various inflammation related ocular diseases in clinical.

Author contributions

LC and DY perform the experiment and analysis the data; LC, DY, NW, QY and HS characterized the material and analysis the data. YP and YF: conceived and supervised the research. All authors discussed the progress of the research and reviewed the manuscript. LC, YP and YF wrote the paper.

Data and materials availability

All data pertaining to the conclusions in this manuscript are present in the main manuscript and/or the Supplementary Materials. Additional relevant data may be requested from the authors.

CRediT authorship contribution statement

Liangbo Chen: Methodology, Software, Data curation, Writing –
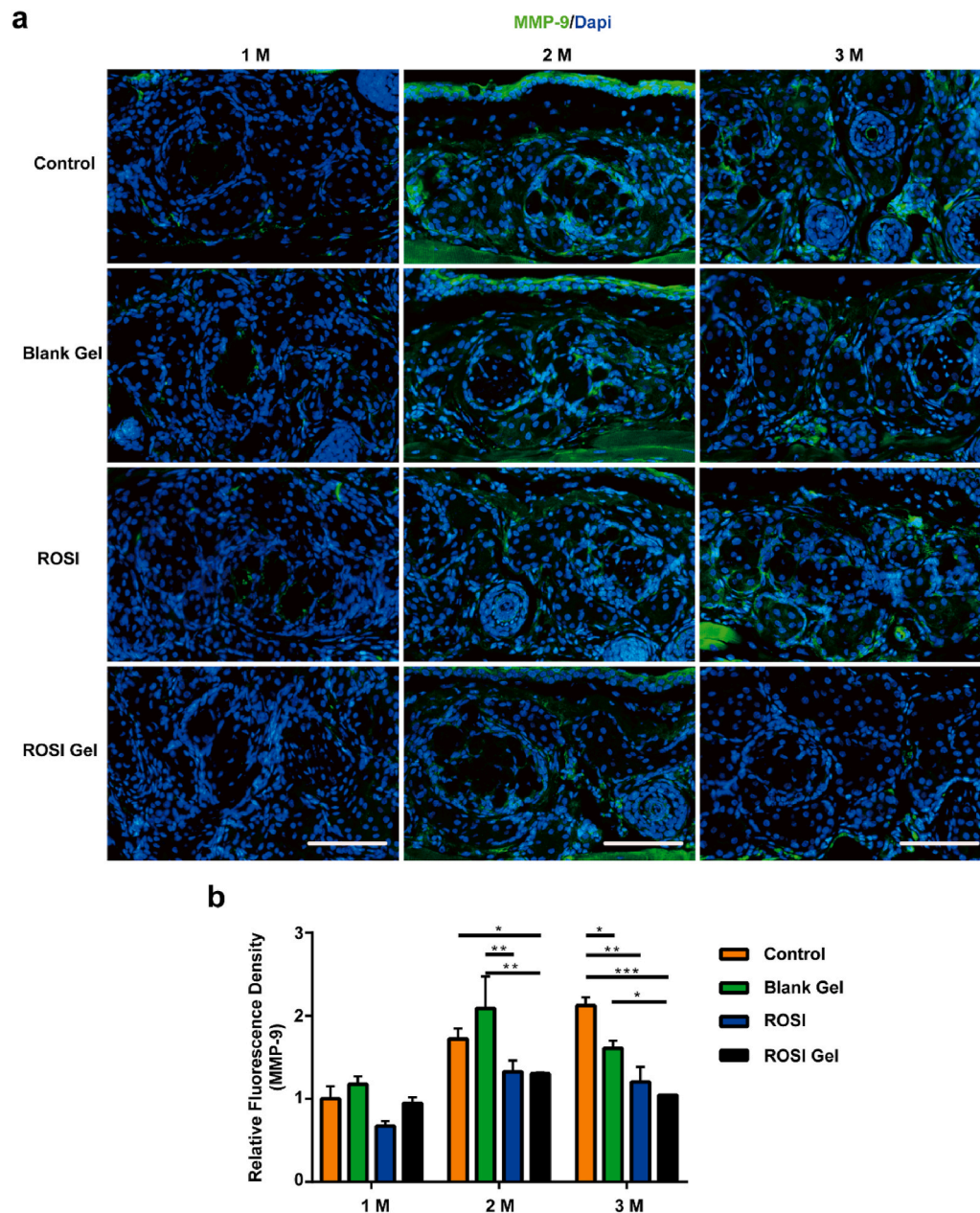
Fig. 7. MMP-9 activity was suppressed by Rosi-hydrogel treatment. (a, b) Representative immunofluorescent images of MMP-9 staining. Immunofluorescence intensity of MMP-9 increased significantly in the Control and Blank Gel groups during aging. On the contrary, Rosi-hydrogel treatment significantly suppressed the expression of MMP-9. *$P < 0.05$, **$P < 0.01$, and ***$P < 0.001$. M indicates month, Scale bar: 100 μm.

original draft, preparation. **Dan Yan:** Methodology, Software, Data curation, Writing – original draft, preparation. **Nianxuan Wu:** Visualization, Investigation. **Qinke Yao:** Visualization, Investigation. **Hao Sun:** Visualization, Investigation. **Yan Pang:** Conceptualization, Writing – review & editing, Supervision. **Yao Fu:** Conceptualization, Writing – review & editing, Supervision.

Declaration of competing interest

All authors declare that they had no competing interests.

Acknowledgments

Appendix A. Supplementary data

Supplementary data to this article can be found online at https://doi.org/10.1016/j.bioactmat.2021.02.040.

References

[1] H. Kaji, N. Nagai, M. Nishizawa, T. Abe, Drug delivery devices for retinal diseases, Adv. Drug Deliv. Rev. 128 (2018) 148–157.

[2] C.Y. Liu, Wakayama Symposium: notch-FoxL2-α-SMA axis in eyelid levator muscle development and congenital blepharophimosis, Ocul. Surf. 10 (2012) 221–223.

[3] T. Suzuki, S. Teramukai, S. Kinoshita, Meibomian glands and ocular surface inflammation, Ocul. Surf. 13 (2015) 133–149.

[4] A.B.D. Grisolia, R.C. Couso, S. Matayoshi, R.S. Douglas, C.A. Briceño, Non-surgical treatment for eyelid retraction in thyroid eye disease (TED), Br. J. Ophthalmol. (2017) bjophthalmol-2017-310695.

[5] J.S. Yoon, S.Y. Lee, Long-term functional and cosmetic outcomes after frontalis suspension using autogenous fascia lata for pediatric congenital ptosis, Ophthalmology 116 (2009) 1405–1414.

[6] J.A. Shields, H. Demirci, B.P. Marr, R.C. Eagle Jr., C.L. Shields, Sebaceous carcinoma of the eyelids: personal experience with 60 cases, Ophthalmology 111 (2004) 2151–2157.

[7] S.C. Pflugfelder, P.M. Karpecki, V.L. Perez, Treatment of blepharitis: recent clinical trials, Ocul. Surf. 12 (2014) 273–284.

[8] S. Cote, A.C. Zhang, V. Ahmadzai, A. Maleken, C. Li, J. Oppedisano, K. Nair, L. Busija, L.E. Downie, Intense pulsed light (IPL) therapy for the treatment of meibomian gland dysfunction, Cochrane Database Syst. Rev. 3 (2020) CD013559.

[9] M.A. Lemp, K.K. Nichols, Blepharitis in the United States 2009: a survey-based perspective on prevalence and treatment, Ocul. Surf. 7 (2009) S1–S14.

[10] K. Lindsley, S. Matsumura, E. Hatef, E.K. Akpek, Interventions for chronic blepharitis, Cochrane Database Syst. Rev. (2012) (2012) CD005556.

[11] T. Meng, V. Kulkarni, R. Simmers, V. Brar, Q. Xu, Therapeutic implications of nanomedicine for ocular drug delivery, Drug Discov. Today 24 (2019) 1524–1538.

[12] Y. Weng, J. Liu, S. Jin, W. Guo, X. Liang, Z. Hu, Nanotechnology-based strategies for treatment of ocular disease, Acta Pharm. Sin. B 7 (2017) 281–291.

[13] Y.H. Weng, X.W. Ma, J. Che, C. Li, J. Liu, S.Z. Chen, Y.Q. Wang, Y.L. Gan, H. Chen, Z.B. Hu, K.H. Nan, X.J. Liang, Nanomicelle-assisted targeted ocular delivery with enhanced antiinflammatory efficacy in vivo, Adv. Sci. 5 (2017) 1700455.

[14] I.P. Kaur, S. Kakkar, Nanotherapy for posterior eye diseases, J. Contr. Release 193 (2014) 100–112.

[15] U. Soiberman, S.P. Kambhampati, T. Wu, M.K. Mishra, Y. Oh, R. Sharma, J. Wang, A.E. Al Towerki, S. Yiu, W.J. Stark, R.M. Kannan, Subconjunctival injectable dendrimer-dexamethasone gel for the treatment of corneal inflammation, Biomaterials 125 (2017) 38–53.

[16] R.J. Noecker, L.A. Herrygers, R. Anwaruddin, Corneal and conjunctival changes caused by commonly used glaucoma medications, Cornea 23 (2004) 490–496.

[17] C. Baudouin, A. Labbé, H. Liang, A. Pauly, F. Brignole-Baudouin, Preservatives in eyedrops: the good, the bad and the ugly, Prog. Retin. Eye Res. 29 (2010) 312–334.

[18] F. Mottaghitalab, M. Farokhi, M.A. Shokrgozar, F. Atyabi, H. Hosseinkhani, Silk fibroin nanoparticle as a novel drug delivery system, J. Contr. Release 206 (2015) 161–176.

[19] M. Farokhi, F. Mottaghitalab, M.A. Shokrgozar, K.L. Ou, C. Mao, H. Hosseinkhani, Importance of dual delivery systems for bone tissue engineering, J. Contr. Release 225 (2016) 152–169.

[20] K.L. Ou, H. Hosseinkhani, Development of 3D in vitro technology for medical applications, Int. J. Mol. Sci. 15 (2014) 17938–17962.

[21] H. Hosseinkhani, 3D in vitro technology for drug discovery, Curr. Drug Saf. 7 (2012) 37–43.

[22] G. Sharifzadeh, H. Hosseinkhani, Biomolecule-responsive hydrogels in medicine, Adv. Healthc. Mater. 6 (2017).

[23] Y. Liu, D. Fan, Novel hyaluronic acid-tyrosine/collagen-based injectable hydrogels as soft filler for tissue engineering, Int. J. Biol. Macromol. 141 (2019) 700–712.

[24] T. Lin, Y. Lu, X. Zhang, L. Gong, C. Wei, Treatment of dry eye by intracanalicular injection of a thermosensitive chitosan-based hydrogel: evaluation of biosafety and availability, Biomater. Sci. 6 (2018) 3160–3169.

[25] L.J. Luo, D.D. Nguyen, J.Y. Lai, Benzoic acid derivative-modified chitosan-g-poly (N-isopropylacrylamide): methoxylation effects and pharmacological treatments of Glaucoma-related neurodegeneration, J. Contr. Release 317 (2020) 246–258.

[26] H. Hosseinkhani, P.D. Hong, D.S. Yu, Self-assembled proteins and peptides for regenerative medicine, Chem. Rev. 113 (2013) 4837–4861.

[27] M. Nowakowska, S. Zapotoczny, M. Sterzel, E. Kot, Novel water-soluble photosensitizers from dextrans, Biomacromolecules 5 (2004) 1009–1014.

[28] R. Mehvar, Dextrans for targeted and sustained delivery of therapeutic and imaging agents, J. Contr. Release 69 (2000) 1–25.

[29] S.W. Kim, Y. Xie, P.Q. Nguyen, V.T. Bui, K. Huynh, J.S. Kang, D.J. Brown, J. V. Jester, PPARγ regulates meibocyte differentiation and lipid synthesis of cultured human meibomian gland epithelial cells (hMGEC), Ocul. Surf. 16 (2018) 463–469.

[30] J. Bu, Y. Wu, X. Cai, N. Jiang, M.V. Jeyalatha, J. Yu, X. He, H. He, Y. Guo, M. Zhang, A.J. Quantock, Z. Liu, W. Li, Hyperlipidemia induces meibomian gland dysfunction, Ocul. Surf. 17 (2019) 777–786.

[31] C.J. Nien, J.R. Paugh, S. Massei, A.J. Wahlert, W.W. Kao, J.V. Jester, Age-related changes in the meibomian gland, Exp. Eye Res. 89 (2009) 1021–1027.

[32] G.J. Parfitt, Y. Xie, M. Geyfman, D.J. Brown, J.V. Jester, Absence of ductal hyper-keratinization in mouse age-related meibomian gland dysfunction (ARMGD), Aging 5 (2013) 825–834.

[33] J.V. Jester, E. Potma, D.J. Brown, PPARγ regulates mouse meibocyte differentiation and lipid synthesis, Ocul. Surf. 14 (2016) 484–494.

[34] J. Chen, C. Yan, M. Zhu, Q. Yao, C. Shao, W. Lu, J. Wang, X. Mo, P. Gu, Y. Fu, X. Fan, Electrospun nanofibrous SF/P(LLA-CL) membrane: a potential substratum for endothelial keratoplasty, Int. J. Nanomed. 10 (2015) 3337–3350.

[35] C. Peng, Y. Wu, X. Ding, D. Chen, C. Zeng, L. Xu, W. Guo, Characteristic cytokine profiles of aqueous humor in glaucoma secondary to sturge-Weber syndrome, Front. Immunol. 11 (2020) 4.

[36] M. Meloni, B. De Servi, D. Marasco, S. Del Prete, Molecular mechanism of ocular surface damage: application to an in vitro dry eye model on human corneal epithelium, Mol. Vis. 17 (2011) 113–126.

[37] C.S. De Paiva, S. Chotikavanich, S.B. Pangelinan, J.D. Pitcher 3rd, B. Fang, X. Zheng, P. Ma, W.J. Farley, K.F. Siemasko, J.Y. Niederkorn, M.E. Stern, D.Q. Li, S. C. Pflugfelder, IL-17 disrupts corneal barrier following desiccating stress, Mucosal Immunol. 2 (2009) 243–253.

[38] J. Xia, Y. Xu, S. Li, W. Sun, K. Yu, W. Tang, Carboxy ester hydrolysis promoted by a zinc(II) 2-[bis(2-aminomethyl)amino]ethanol complex: a new model for indirect activation on the serine nucleophile by zinc(II) in zinc enzymes, Inorg. Chem. 40 (2001) 2394–2401.

[39] R.P. Verma, C. Hansch, Matrix metalloproteinases (MMPs): chemical-biological functions and (Q)SARs, Bioorg. Med. Chem. 15 (2007) 2223–2268.

[40] B.P. Purcell, D. Lobb, M.B. Charati, S.M. Dorsey, R.J. Wade, K.N. Zellars, H. Doviak, S. Pettaway, C.B. Logdon, J.A. Shuman, P.D. Freels, J.H. Gorman 3rd, R. C. Gorman, F.G. Spinale, J.A. Burdick, Injectable and bioresponsive hydrogels for on-demand matrix metalloproteinase inhibition, Nat. Mater. 13 (2014) 653–661.

[41] T. Gajanayake, R. Olariu, F.M. Leclère, A. Dhayani, Z. Yang, A.K. Bongoni, Y. Banz, M.A. Constantinescu, J.M. Karp, P.K. Vemula, R. Rieben, E. Vögelin, A single localized dose of enzyme-responsive hydrogel improves long-term survival of a vascularized composite allograft, Sci. Transl. Med. 6 (2014) 249ra110.

[42] N. Joshi, J. Yan, S. Levy, S. Bhagchandani, K.V. Slaughter, N.E. Sherman, J. Amirault, Y. Wang, L. Riegel, X. He, T.S. Rui, M. Valic, P.K. Vemula, O. R. Miranda, O. Levy, E.M. Gravallese, A.O. Aliprantis, J. Ermann, J.M. Karp, Towards an arthritis flare-responsive drug delivery system, Nat. Commun. 9 (2018) 1275.

[43] A. Tomlinson, A.J. Bron, D.R. Korb, S. Amano, J.R. Paugh, E.I. Pearce, R. Yee, N. Yokoi, R. Arita, M. Dogru, The international workshop on meibomian gland dysfunction: report of the diagnosis subcommittee, Invest. Ophthalmol. Vis. Sci. 52 (2011) 2006–2049.

[44] B. Miljanović, R. Dana, D.A. Sullivan, D.A. Schaumberg, Impact of dry eye syndrome on vision-related quality of life, Am. J. Ophthalmol. 143 (2007) 409–415.

[45] A. Denoyer, G. Rabut, C. Baudouin, Tear film aberration dynamics and vision-related quality of life in patients with dry eye disease, Ophthalmology 119 (2012) 1811–1818.

[46] N.J. Reyes, C. Yu, R. Mathew, C.M. Kunnen, J. Kalnitsky, R.L. Redfern, A. Leonardi, V.L. Perez, A.S. MacLeod, P.K. Gupta, D.R. Saban, Neutrophils cause obstruction of eyelid sebaceous glands in inflammatory eye disease in mice, Sci. Transl. Med. 10 (2018), eaas9164.

[47] Y. Yin, L. Gong, Reversibility of gland dropout and significance of eyelid hygiene treatment in meibomian gland dysfunction, Cornea 36 (2017) 332–337.

[48] G.N. Foulks, A.J. Bron, Meibomian gland dysfunction: a clinical scheme for description, diagnosis, classification, and grading, Ocul. Surf. 1 (2003) 107–126.

[49] S. Yurttaser Ocak, S. Karakus, O.B. Ocak, A. Cakir, S. Bolukbasi, B. Erden, E. Bas, M. Elcioglu, Intense pulse light therapy treatment for refractory dry eye disease due to meibomian gland dysfunction, Int. Ophthalmol. 40 (2020) 1135–1141.

[50] J.J. Qiu, T. Sun, S.H. Fu, Y.F. Yu, Z.P. You, Q. Zhang, F. Liu, J.Q. Huang, Z. H. Wang, A study of dry eye after cataract surgery in MGD patients, Int. Ophthalmol. 40 (2020) 1277–1284.

[51] J. Tauber, A 6-week, prospective, randomized, single-masked study of lifitegrast ophthalmic solution 5% versus thermal pulsation procedure for treatment of inflammatory meibomian gland dysfunction, Cornea 39 (2020) 403–407.

[52] N.R. Trivedi, Z. Cong, A.M. Nelson, A.J. Albert, L.L. Rosamilia, S. Sivarajah, K. L. Gilliland, W. Liu, D.T. Mauger, R.A. Gabbay, D.M. Thiboutot, Peroxisome proliferator-activated receptors increase human sebum production, J. Invest. Dermatol. 126 (2006) 2002–2009.

[53] J.S. Wu, H.D. Tsai, W.M. Cheung, C.Y. Hsu, T.N. Lin, PPAR-γ ameliorates neuronal apoptosis and ischemic brain injury via suppressing NF-κB-Driven p22phox transcription, Mol. Neurobiol. 53 (2016) 3626–3645.

[54] P. Chhadva, R. Goldhardt, A. Galor, Meibomian gland disease: the role of gland dysfunction in dry eye disease, Ophthalmology 124 (2017) S20–S26.

[55] R.G. Baker, M.S. Hayden, S. Ghosh, NF-κB, inflammation, and metabolic disease, Cell Metabol. 13 (2011) 11–22.

[56] Q. Li, I.M. Verma, NF-kappaB regulation in the immune system, Nat. Rev. Immunol. 2 (2002) 725–734.

[57] J. Mauris, J. Dieckow, S. Schob, B. Pulli, M.P. Hatton, S. Jeong, A. Bauskar, E. Gabison, R. Nowak, P. Argüeso, Loss of CD147 results in impaired epithelial cell differentiation and malformation of the meibomian gland, Cell Death Dis. 6 (2015), e1726.

[58] T. Sakimoto, M. Sawa, Metalloproteinases in corneal diseases: degradation and processing, Cornea 31 (Suppl 1) (2012) S50–S56.